SUPPORTING INFORMATION

Organic cations in halide perovskite solid solutions: exploring beyond size effects

F. B. Minussi[1*], R. M. Silva Jr.[2], J. C. S. Moraes[1], E. B. Araújo[1]

[1] Department of Physics and Chemistry, São Paulo State University, 15385-007, Ilha Solteira, SP - Brazil

[2] Department of Electrical Engineering, São Paulo State University, 15385-007, Ilha Solteira, SP - Brazil

CONTENTS

[*] corresponding author: fbminussi@gmail.com

Supplementary Note 1: Precursor and perovskite masses

Table S1 - Weighted reaction precursors and resulting perovskite (HP) masses. Yield is the ratio between the HP obtained and expected (sum of precursors) masses.

Composition	PbI_2 (g)	MAI (g)	GAI (g)	EAI (g)	ACI (g)	HP (g)	Yield (%)
MAPI	0.901_9	0.310_6	0	0	0	1.085_0	89.5
GA0.1	0.897_1	0.278_5	0.036_0	0	0	1.118_7	92.3
EA0.1	0.899_3	0.279_1	0	0.034_1	0	1.109_5	91.5
AC0.1	0.898_5	0.278_3	0	0	0.036_0	1.088_0	89.7

Supplementary Note 2: Setup for the light-accelerated degradation test

Figure S1 - Home-made setup used for the light-accelerated degradation test. The samples were distributed uniformly in the Petri dish, which was positioned in the center of the rotating (6 Hz clockwise) platform and submitted to direct and mirror-reflected illumination from the LED lamp. The lamp specifications are a power of 6 W, luminous flux of 560 lm, and color cold white (6500 K). The box (30 x 20 x 15 cm) remained closed and sealed with masking tape during the test. Inside humidity was kept as low as possible by drying silica beads. Temperature and relative humidity were constantly monitored.

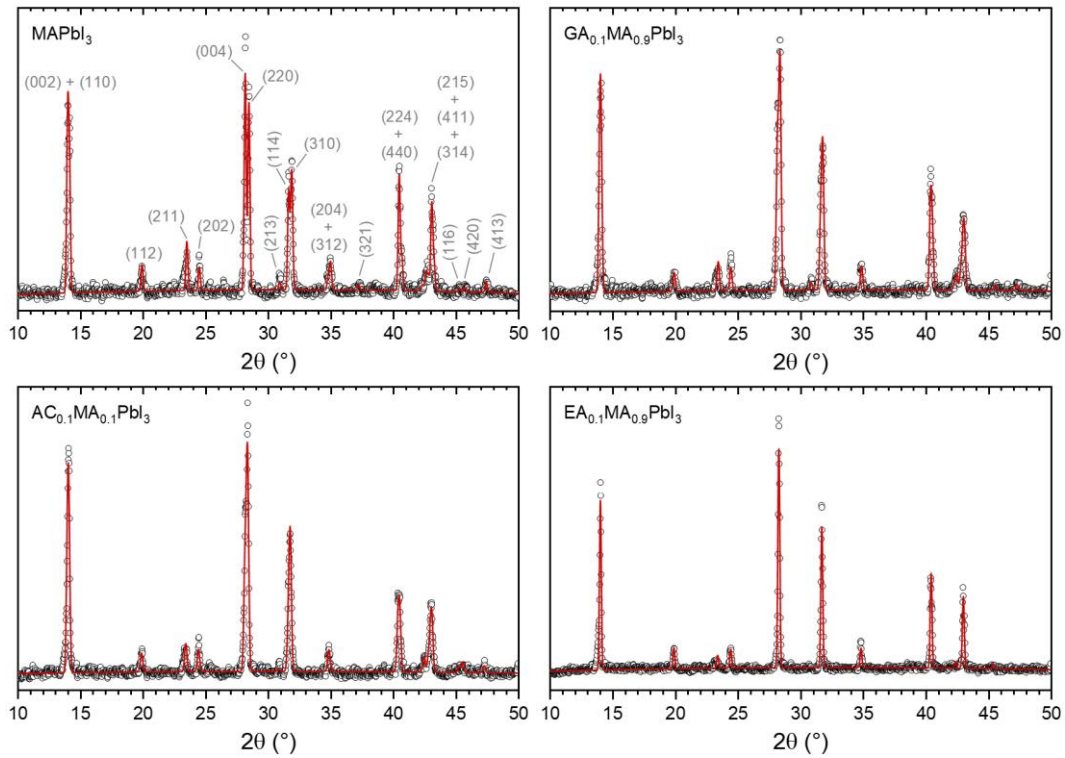# Supplementary Note 3: Le Bail fits of XRD data

Figure S2 - Experimental data (black dots) and Le Bail fits (red lines) of studied compositions. Fits were calculated using the WinPLOTR package as implemented in the Fullprof software (version of April 2024) considering the $I4cm$ (tetragonal) space groups.

Table S2 - Original lattice parameters obtained through the Le Bail fit.

Composition	a (Å)	c (Å)	χ^2
MAPbI$_3$	8.8599 ± 0.0005	12.6600 ± 0.0007	1.75
GA$_{0.1}$MA$_{0.9}$PbI$_3$	8.8879 ± 0.0005	12.6603 ± 0.0011	1.47
AC$_{0.1}$MA$_{0.9}$PbI$_3$	8.8905 ± 0.0005	12.6594 ± 0.0014	1.35
EA$_{0.1}$MA$_{0.9}$PbI$_3$	8.9067 ± 0.0006	12.6184 ± 0.0011	1.63

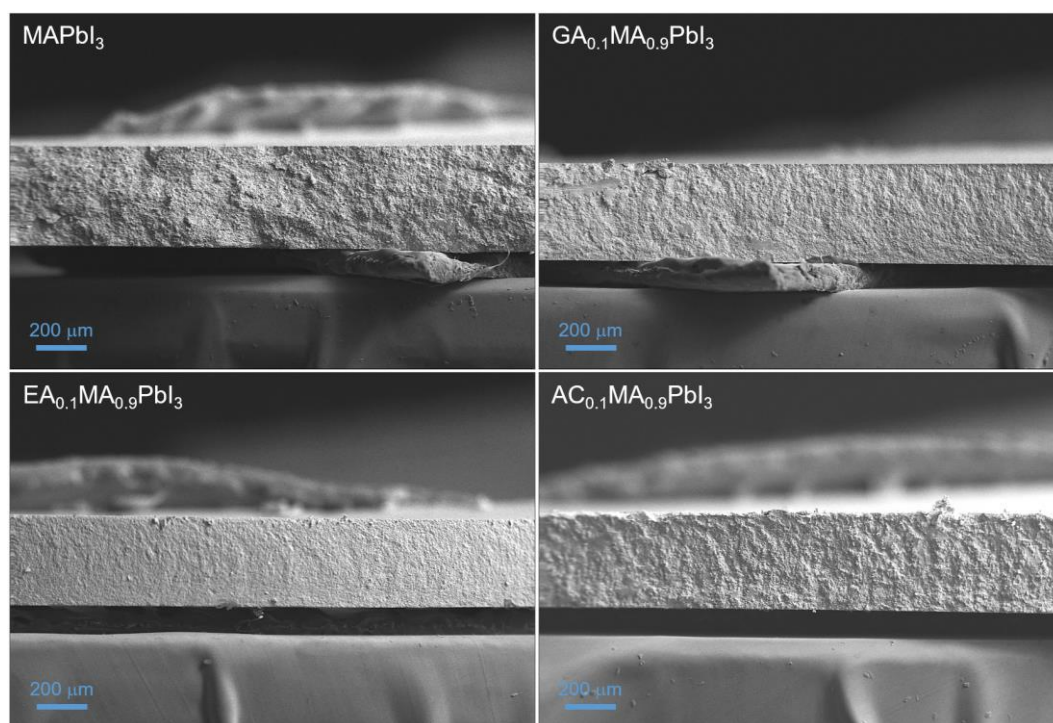# Supplementary Note 4: Thickness of samples

Figure S3 - Cross-section SEM images of the samples used in the electrical characterizations.

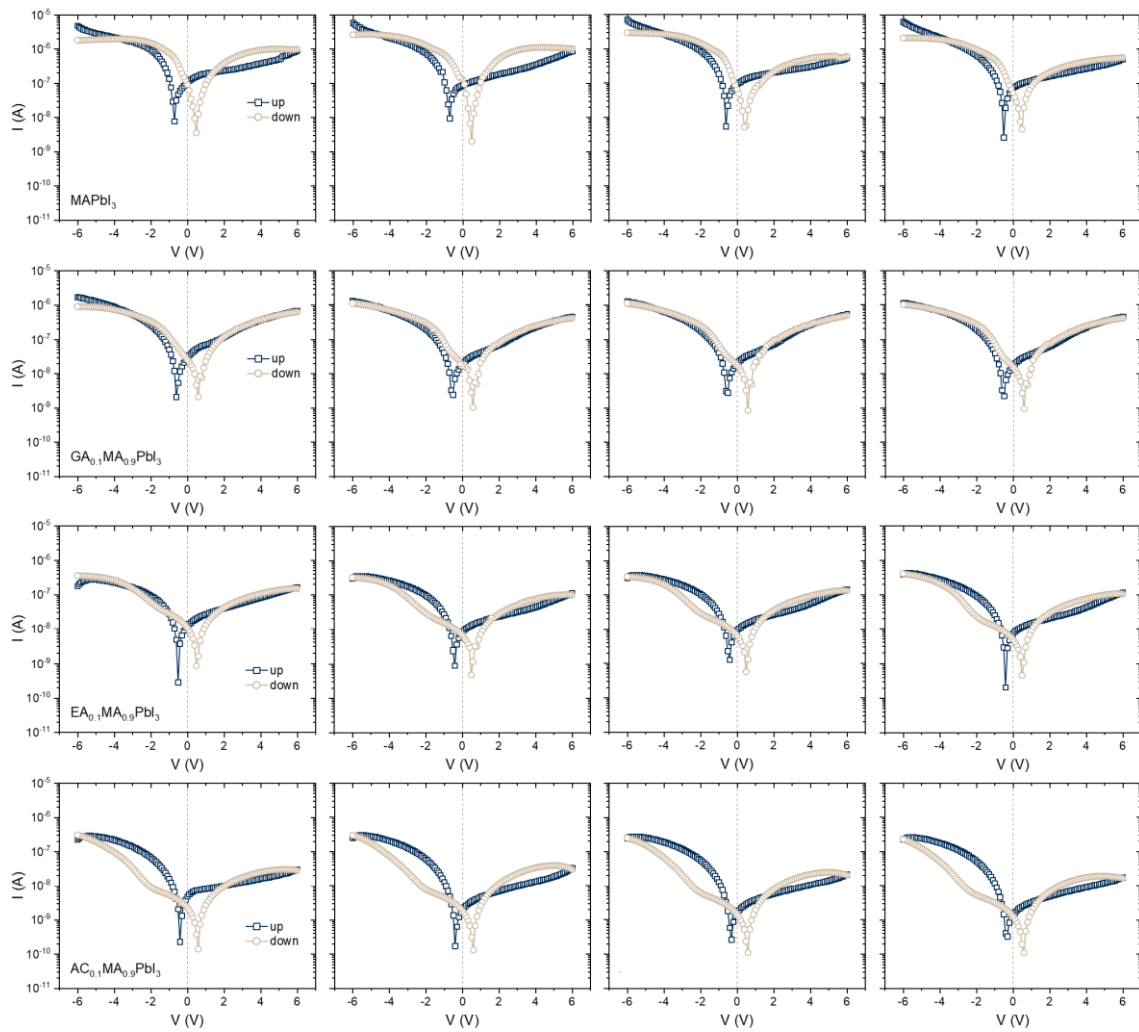# Supplementary Note 5: Measurements for *I-V* hysteresis

Figure S4 - Four measurements of up and down cycles with a scan rate of 0.1 V s^{-1} used to evaluate the *I-V* hysteresis.

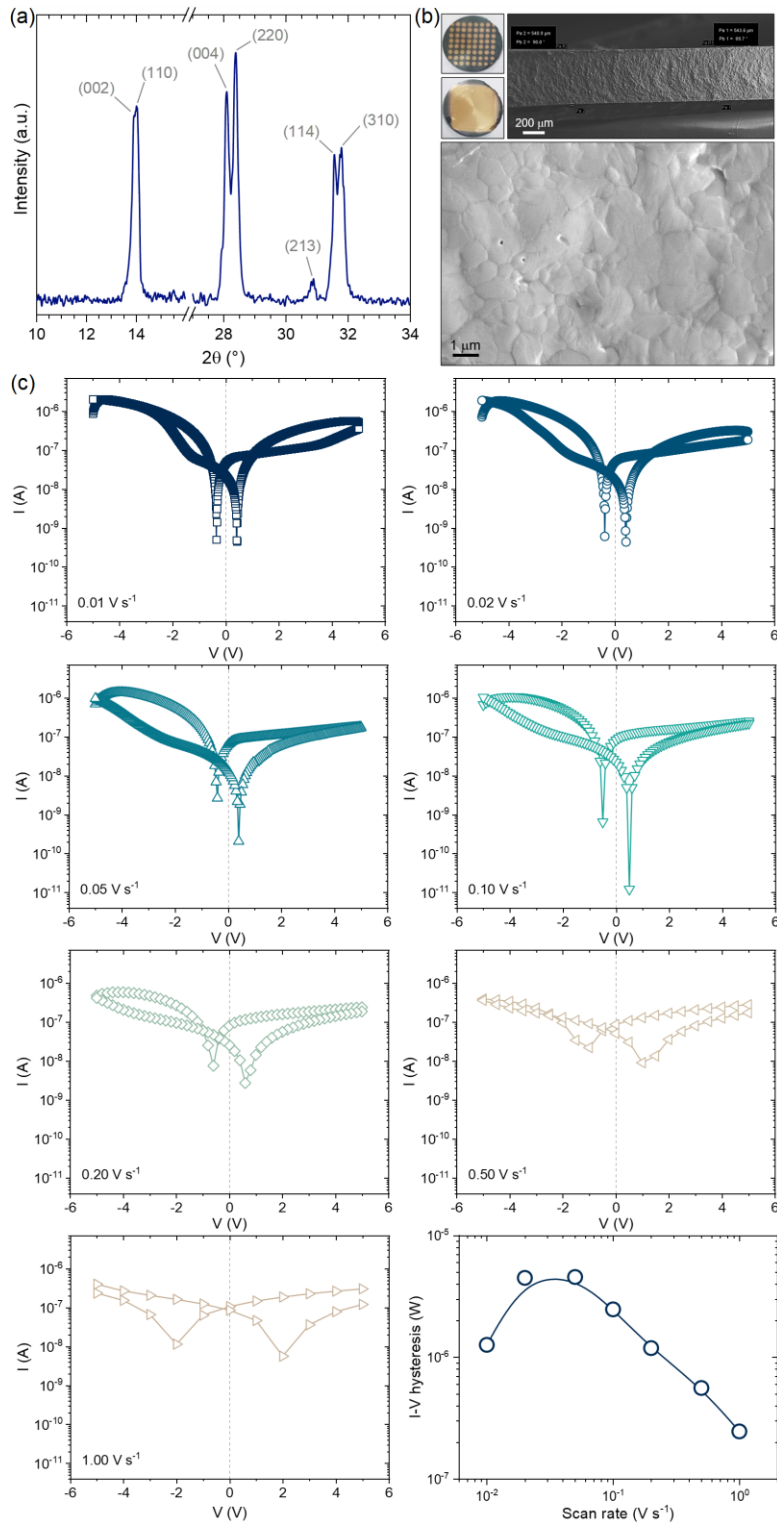**Supplementary Note 6: Dependence of the *I-V* hysteresis on scan rate**

Figure S5 - (a) XRD of another MAPbI$_3$ sample synthesized to evaluate the effect of the scan rate on the *I-V* hysteresis. (b) Photograph of the sample with deposited gold electrodes and SEM images of its surface and cross-section. (c) Up and down cycles were measured at different scan rates from 0.01 to 1.00 V s^{-1} and the *I-V* hysteresis values as a function of the scan rates. The measurements were performed at the same electrode with intervals of more 40 minutes between cycles, starting from higher to lower scan rates.

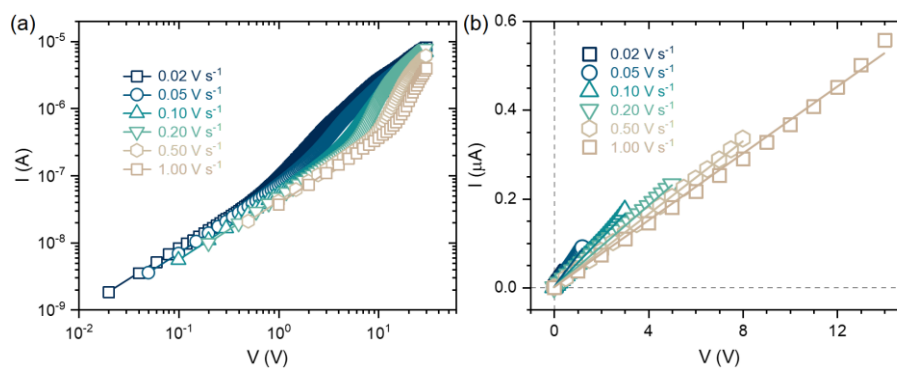## Supplementary Note 7: Dependence of the *I-V* forward curves on scan rate

Figure S6 - (a) *I-V* curves measured with different scan rates. (b) Detail of the low voltage region where the conduction follows an ohmic behavior. The ohmic conductivity is proportional to the slope of lines, i.e., the apparent conductivity increases the lower the scan rate. On the other hand, the deviation from the ohmic regime occurs at lower voltages. All measurements were performed at the sample shown previously and at the same electrode (but different from the one used to collect the data of *I-V* cycles), with intervals of more than 40 minutes between cycles, starting from higher to lower scan rates.

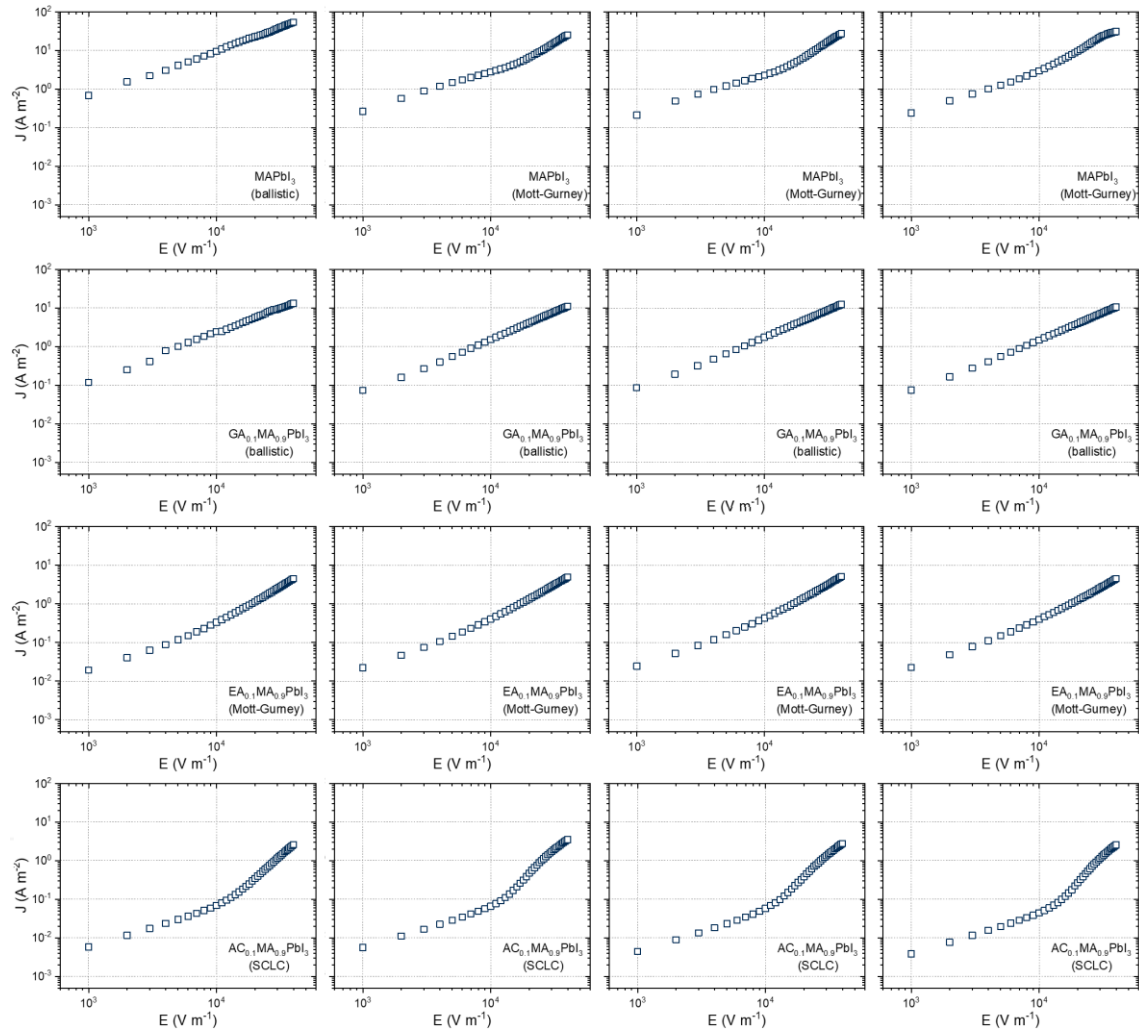## Supplementary Note 8: Forward *I-V* measurements

Figure S7 - Four forward measurements with a scan rate of 0.5 V s^{-1} used to evaluate the electronic carrier in samples of each composition.

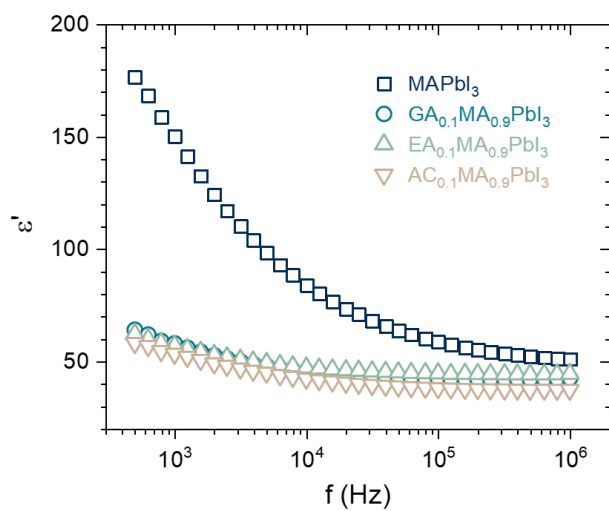**Supplementary Note 9: Frequency-dependent dielectric permittivity**

Figure S8 - Real part of the dielectric permittivity as a function of frequency measured from 5.10^2 to 10^6 Hz at room temperature.

Supplementary Note 10: Electronic carrier parameters

Table S3 - Summary of experimental data, models used, and evaluated electronic charge carrier parameters of samples. The n_e values were calculated using the relation $\sigma_{ohmic} = q\mu_e n_e$.

Composition	ε' (at 1 MHz)	σ_{ohmic} (10^{-6} S m^{-1})	Model	μ_e (10^{-3} m^2 V^{-1} s^{-1})	n_e (10^{16} m^{-3})
MAPbI$_3$	51	784	Ballistic	60	8.1
		294	Mott-Gurney	17	11
		243	Mott-Gurney	19	8.0
		251	Mott-Gurney	30	5.2
GA0.1	42	183	Ballistic	24	4.8
		101	Ballistic	19	3.3
		120	Ballistic	21	3.5
		102	Ballistic	18	3.5
EA0.1	44	22.4	Mott-Gurney	3.0	4.6
		27.0	Mott-Gurney	3.4	5.0
		29.8	Mott-Gurney	3.5	5.3
		28.0	Mott-Gurney	3.1	5.7
AC0.1	37	5.89	SCLC	1.8	2.0
		5.65	SCLC	2.7	1.3
		4.57	SCLC	1.9	1.5
		3.90	SCLC	1.7	1.4

Supplementary Note 11: Changes in precursor organic salts exposed to ambient air
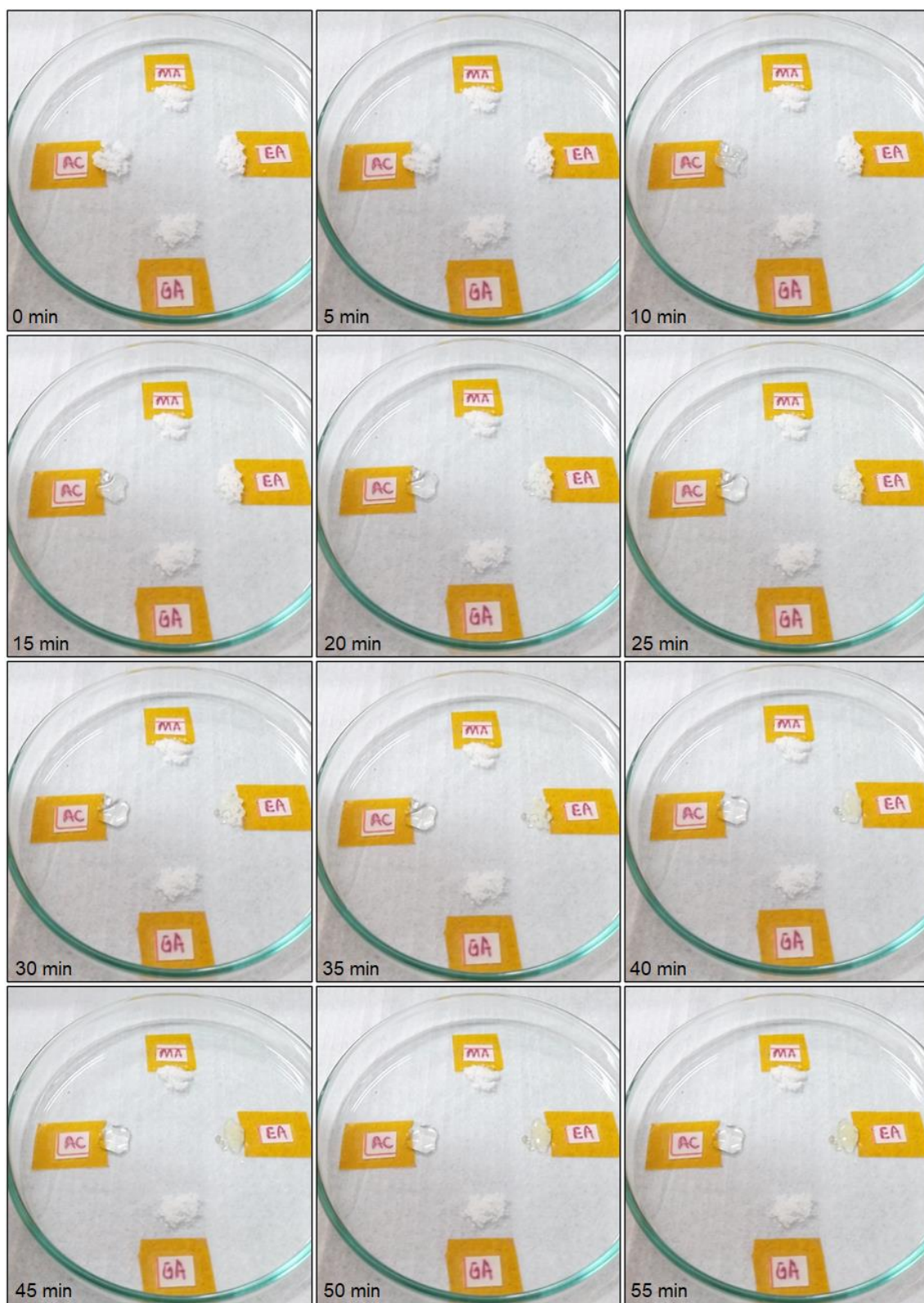

Figure S9 - Changes to visual aspect of portions of precursor MAI, EAI, GAI, and ACI powders with time when exposed to ambient air. MA, EA, GA, and AC are the positions of respective iodine salts. Tapes with the designation of organic cation salts are under the Petri dish.